nature physics

ARTICLES

PUBLISHED ONLINE: 22 MAY 2017 | DOI: 10.1038/NPHYS4119

Measuring out-of-time-order correlations and multiple quantum spectra in a trapped-ion quantum magnet

Martin Gärttner[1†], Justin G. Bohnet[2†], Arghavan Safavi-Naini[1], Michael L. Wall[1], John J. Bollinger[2] and Ana Maria Rey[1*]

Controllable arrays of ions and ultracold atoms can simulate complex many-body phenomena and may provide insights into unsolved problems in modern science. To this end, experimentally feasible protocols for quantifying the buildup of quantum correlations and coherence are needed, as performing full state tomography does not scale favourably with the number of particles. Here we develop and experimentally demonstrate such a protocol, which uses time reversal of the many-body dynamics to measure out-of-time-order correlation functions (OTOCs) in a long-range Ising spin quantum simulator with more than 100 ions in a Penning trap. By measuring a family of OTOCs as a function of a tunable parameter we obtain fine-grained information about the state of the system encoded in the multiple quantum coherence spectrum, extract the quantum state purity, and demonstrate the buildup of up to 8-body correlations. Future applications of this protocol could enable studies of many-body localization, quantum phase transitions, and tests of the holographic duality between quantum and gravitational systems.

Time reversal has fascinated and puzzled physicists for centuries. In an iconic example, Josef Loschmidt argued that the second law of thermodynamics would be violated by time-reversing an entropy-increasing collision[1]. Ludwig Boltzmann responded by formulating the probabilistic definition of entropy, one of the cornerstones of statistical mechanics, and now a fundamental concept in quantum information. Since the days of Boltzmann and Loschmidt, the notion of time reversal has moved from the arena of thought experiments into the laboratory, with time reversal of non-interacting quantum systems in the form of Hahn spin echoes[2] forming an essential part of nuclear magnetic resonance (NMR)[3] and magnetic resonance imaging.

Recently, the experimental implementation of many-body time-reversal protocols[4,5] in atomic quantum systems has attracted attention[6–9] for their potential to quantify the flow of quantum information in time and set bounds on thermalization times[10–13], which might also enable experimental tests of the holographic duality between quantum and gravitational systems[6,14–17]. The key quantities sought after are special types of out-of-time-order correlation (OTOC) functions,

$$F(\tau) = \langle \hat{W}^{\dagger}(\tau)\hat{V}^{\dagger}\hat{W}(\tau)\hat{V}\rangle \tag{1}$$

where $\hat{W}(\tau) = e^{i\hat{H}\tau}\hat{W}e^{-i\hat{H}\tau}$, with $\hat{H}$ an interacting many-body Hamiltonian and $\hat{W}$ and $\hat{V}$ two commuting unitary operators. Physically, $F(\tau)$ measures the 'scrambling' of quantum information across the system's many-body degrees of freedom—for example, how fast an initial local perturbation becomes inaccessible to local probes[16]. Since $\mathrm{Re}[F(\tau)] = 1 - \langle|[\hat{W}(\tau), \hat{V}]|^2\rangle/2$, $F(\tau)$ encapsulates the degree by which the initially commuting operators $\hat{W}$ and $\hat{V}$ fail to commute at later times due to the interactions generated by $\hat{H}$, which we adopt as an operational definition of scrambling.

Most theoretical studies of scrambling have focused on so-called fast scramblers in thermal states[10,11,16], systems where the commutator grows exponentially at a rate exclusively determined by the temperature. However, the scrambling behaviour of non-equilibrium systems at zero temperature will depend on the microscopic parameters of the Hamiltonian. This largely unexplored topic can provide valuable insights into the dynamics of interacting quantum many-body systems.

Here we perform measurements of OTOCs with a quantum simulator composed of more than 100 trapped ions[18] interacting via all-to-all Ising interactions that can be reversed in time. This Ising interaction allows us to study interesting entangled states[18–21], yet still operate in a regime where simulations on conventional computers are feasible. Thus, our work is a first stepping stone for exploring scrambling in initially pure quantum systems. Our approach is modelled after the multiple quantum coherence (MQC) protocol developed in the context of NMR[3,22,23] to quantify the buildup of multi-particle coherences (off-diagonal elements of the many-body density matrix). We show that this protocol, under specific choices of the initial state (pure states in our experiment), implements the measurement of a family of OTOCs. Careful comparison with theory allows us to use the measurements as a verification protocol to benchmark the performance of the quantum simulator, and to sensitively quantify different sources of decoherence and imperfect control. In our experiment, which starts with a pure product state, scrambling can be physically interpreted as the process by which the information stored (or encoded) in the initial state, through the interactions, is distributed over and therefore stored in other many-body degrees of freedom of the

[1]JILA, NIST and Department of Physics, University of Colorado, 440 UCB, Boulder, Colorado 80309, USA. [2]National Institute of Standards and Technology (NIST), Boulder, Colorado 80305, USA. †These authors contributed equally to this work. *e-mail: arey@jila.colorado.edu

system. Thus, it cannot be extracted by measurements of single-particle observables. Instead it requires measurements of higher-order correlations. The information is not lost, but requires reading out the various degrees of freedom.

Future generalizations such as adding a spatially inhomogeneous magnetic field or a periodic drive would allow one to experimentally study scrambling behaviour in regimes intractable to theory, to explore the possibility of fast scrambling in low-temperature systems, and to investigate possible connections between chaos and fast scrambling away from the semi-classical limit. The protocols demonstrated here are widely applicable, and could be implemented in a variety of other platforms with reversible dynamics, such as linear ion chains[20,24], ultracold atomic gases[4,5,25], cold atoms in optical cavities[26–28], Rydberg-dressed atoms[29], superconducting qubits[30], and NMR systems[22].

The general protocol is illustrated in Fig. 1a. For concreteness, we consider the system of spin-1/2s, which we implement in our trapped-ion experiment. The state of interest $\hat{\rho}(\tau)$ is prepared by evolving a fiducial state, $\hat{\rho}_0$, under an interacting Hamiltonian $\hat{H}$ for a time τ. In our experiment the initial density matrix is $\hat{\rho}_0 = |+\ldots+\rangle\langle+\ldots+|$, where $|+\rangle = (|\uparrow\rangle + |\downarrow\rangle)/\sqrt{2}$ and $\hat{H}$ is a collective Ising model given by

$$\hat{H}_{zz} = \frac{J}{N}\sum_{i<j}\hat{\sigma}_i^z\hat{\sigma}_j^z \tag{2}$$

where N is the number of spins and $\hat{\sigma}_i^z$ are Pauli spin operators. Inverting the sign of $\hat{H}_{zz}$ (by changing J to $-J$) and evolving again for time τ to the final state $\hat{\rho}_f$, implements the many-body time reversal, which ideally takes the system back to the initial state $\hat{\rho}_0$. If a state rotation $\hat{R}_x(\phi) = e^{-i\hat{S}_x\phi}$, here about the x-axis with $\hat{S}_x = \frac{1}{2}\sum_i\hat{\sigma}_i^x$, is inserted between the two halves of the time evolution through a variable angle ϕ, the dependence of the revival probability on this angle contains information about $\hat{\rho}(\tau)$. In this work, we measure two different observables at the end of the sequence, the collective magnetization along the x-direction, $\langle\hat{S}_x\rangle = \mathrm{tr}[\hat{S}_x\hat{\rho}_f]$, and the fidelity $\mathcal{F}_\phi(\tau) = \mathrm{tr}[\hat{\rho}_0\hat{\rho}_f]$.

The magnetization provides a direct measurement of

$$\frac{2}{N}\langle\hat{S}_x\rangle = F_\phi(\tau) = \langle\hat{W}_\phi^\dagger(\tau)\hat{\sigma}_i^x\hat{W}_\phi(\tau)\hat{\sigma}_i^x\rangle_0 \tag{3}$$

for any i, with $\hat{W}_\phi(\tau) = e^{i\hat{H}_{zz}\tau}\hat{R}_x(\phi)e^{-i\hat{H}_{zz}\tau}$. Here, $\langle\cdot\rangle_0$ denotes the expectation value in state $\hat{\rho}_0$. The implementation is facilitated by the fact that $\hat{V}|+\rangle = \hat{\sigma}_i^x|+\rangle = |+\rangle$. Moreover, single-spin resolution is not necessary due to the permutation symmetry of our system that directly maps $\hat{\sigma}_i^x$ to the global magnetization along x: $\hat{\sigma}_i^x \to (2/N)\hat{S}_x$. In the absence of permutation symmetry, the OTOC measured by $F_\phi(\tau)$ should be interpreted as the average over the magnetization of each of the spins in the array.

Similarly, the fidelity, that is, many-body overlap with the initial state, can be cast as an OTOC, where now $\hat{V} = \hat{\rho}_0$ is not unitary but $\mathcal{F}_\phi(\tau)$ still measures the failure of two operators to commute following dynamical evolution (see Methods). Moreover, the fidelity can be directly linked to the so-called multiple quantum intensities I_m (see Methods), which quantify the amplitudes of the off-diagonal elements[3], or coherences, of the density matrix $\hat{\rho}(\tau)$. The I_m are measured by the Fourier components of

$$\mathcal{F}_\phi(\tau) = \mathrm{tr}[\hat{\rho}_f\hat{\rho}_0] = \mathrm{tr}[\hat{\rho}(\tau)\hat{\rho}_\phi(\tau)] = \sum_{m=-N}^{N} I_m(\tau)e^{-im\phi} \tag{4}$$

where $\hat{\rho}_\phi(\tau) = \hat{R}_x(\phi)\hat{\rho}(\tau)\hat{R}_x^\dagger(\phi)$ (see Methods). In contrast to previous implementations in NMR spectroscopy, which typically operate at effectively infinite temperature, here we consider a spin system that is initially in a pure state at zero temperature.

Beyond the expected decay of the measured OTOCs for increasing τ and fixed ϕ, studying the dependence of them on the rotation angle ϕ thus reveals information about the buildup of correlations and provides fine-grained information about the many-body properties of the state $\hat{\rho}(\tau)$. The value of the fidelity at $\phi = 0 \bmod 2\pi$ also provides a direct measurement of the purity of the many-body spin state, $\mathcal{F}_0(\tau) = \mathrm{tr}[\hat{\rho}(\tau)^2]$. Note that the fidelity measurement directly implements a many-body Loschmidt echo, which is typically challenging to experimentally measure for systems of more than $\sim$10 particles.

To clearly illustrate the dynamics of I_m and their connection to off-diagonal elements of the density matrix, we compute $\mathcal{F}_\phi(\tau)$ for a small system with $N = 6$ spins shown in Fig. 1b,c. At $\tau = t_{\mathrm{cat}} = \pi\hbar N/(4J)$ a macroscopic superposition (Schrödinger cat) state along x is formed[31], which is signalled in the MQC spectrum by the cancellation of all I_m except I_0 and $I_{\pm N}$. Note that for this case our scheme is equivalent to the interferometric cat-state verification scheme realized with $N \leq 6$ ions in Paul traps[19].

Motivated by the MQC protocol we study the dynamics of the Fourier amplitudes A_m of the magnetization

$$F_\phi(\tau) = \sum_{m=-N}^{N} A_m(\tau)e^{-im\phi} \tag{5}$$

which probe the buildup of many-body correlations. One can show that a non-zero $A_m(\tau)$ signals the buildup of at least m-body correlations. In the case of the Ising model, where all terms in the Hamiltonian commute with each other, $A_m(\tau)$ can only be non-zero if the Hamiltonian directly couples a given spin to $m-1$ other spins (see Methods and Supplementary Information). In Fig. 1d we illustrate the I_m and A_m dynamics for $N = 48$ in the absence of decoherence, showing the sequential buildup of higher-order coherences and correlations. Even for the homogeneous Ising interaction, the protocol reveals a rich structure in the many-body state, including multiple revivals of coherences. The I_m spread more rapidly than the A_m because the I_m depends on the many-body overlap with the initial state, an N-body operator, which is more sensitive to the central rotation than the mean spin, a single-body observable.

Our experimental demonstration uses two-dimensional (2D) arrays of laser-cooled $^9Be^+$ ions in a Penning trap, where the spins are the valence electron spin states in the $B = 4.46$ T magnetic field[18,32,33]. Arbitrary collective spin rotations are applied via microwave pulses (see Fig. 2 and Supplementary Information). Long-range, tunable spin interactions are engineered through a time-dependent optical dipole force (ODF), characterized by a frequency μ_r, that couples the spins to the axial motional (phonon) modes of the ion crystal. The driven spin-dependent motion, combined with the Coulomb force, mediates the spin–spin interaction. Laser cooling and optical pumping allow us to initialize the spins in a pure, coherent collective spin state with fidelity >99.9% (ref. 34), and initialize the motional modes with an average thermal occupation of six quanta, set by the Doppler cooling limit.

To implement the reversible Ising dynamics, we operate in a regime where the spins couple to a single phonon mode, the collective centre-of-mass (COM) mode at frequency ω_z. Although there are N axial phonon modes in the crystal, the COM mode is well-resolved for the ODF detuning from the COM mode $\delta = \mu_r - \omega_z$ used here[33], justifying the single-mode approximation. Then the spin–phonon dynamics are given by[31,35]

$$\hat{H}_I = -\frac{\Omega_0}{2\sqrt{N}}\sum_{j=1}^{N}\left(\hat{a}_0e^{i\delta\tau} + \hat{a}_0^\dagger e^{-i\delta\tau}\right)\hat{\sigma}_j^z \tag{6}$$

where Ω_0 is proportional to the ODF and $\hat{a}_0(\hat{a}_0^\dagger)$ is the annihilation(creation) operator for the COM mode phonons. In general, the spins will be coupled to the phonon mode, except at

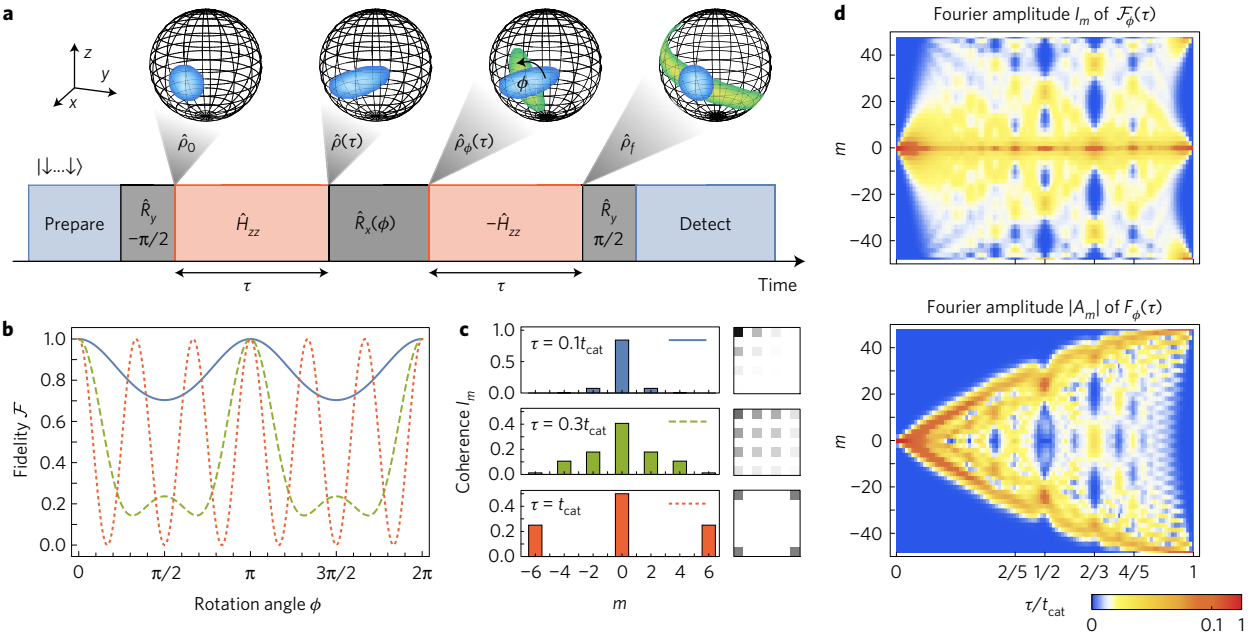

Figure 1 | Illustration of the many-body echo scheme. a, Experimental sequence. The global $-\pi/2$ rotation $\hat{R}_y$ about the y-axis prepares an initial state with all spins pointing along the x-axis, and enables a measurement in this same basis. The generalized Bloch spheres illustrate the evolution of the state (Husimi distribution). In the case of $\phi = 0$ (blue) the spins return to the initial state, while for $\phi = \pi/2$ (green) the overlap of the final state $\hat{\rho}_f$ with the initial state is small. **b**, Fidelity signal for an idealized case with $N = 6$ spins and different evolution times τ given in **c**. **c**, The Fourier transforms of the fidelity signals of **b**. The Fourier amplitudes are identical to the MQCs I_m, which quantify the coherence of the state $\hat{\rho}(\tau)$. The small squares on the right show the absolute values of the density matrix elements of $\hat{\rho}(\tau)$ in the basis of symmetric Dicke states. Thus, I_m is the sum of the squares of all matrix elements at a distance m from the diagonal. The times are given in units of the time to reach the Schrödinger cat state $t_{cat} = \pi\hbar N/(4J)$. **d**, Simulated dynamics of the Fourier amplitudes of fidelity, I_m, and magnetization, A_m, for purely coherent evolution of 48 ions, illustrating complementary probes of the flow of quantum information. The vanishing odd Fourier components are not shown.

particular decoupling times $\tau_n = 2\pi n/\delta$ for an integer n (Fig. 2c and Supplementary Information). Here we always choose $|\delta| = 2\pi n/\tau$, ensuring spins and phonons decouple. This guarantees that the dynamics matches that of the Ising Hamiltonian in equation (2) with uniform couplings $J(\delta)/\hbar = \Omega_0^2/(2\delta)$, and leads to different values of the coupling constant J at different interaction times τ. The detuning-dependent coupling enables us to implement a many-body echo of the spin dynamics by inverting the sign of δ.

For measuring magnetization and fidelity, we collect the global ion fluorescence scattered from the Doppler cooling laser on the cycling transition for ions in $|\uparrow\rangle$, after applying a $\pi/2$ rotation of the spins. We count the total number of photons collected on a photomultiplier tube (PMT) in a detection period, typically $t_c = 5$ ms. From the independently calibrated photons collected per ion, we can infer the state populations, $N_\uparrow$ and $N_\downarrow$. After averaging over many experimental trials, between 500 and 800, we calculate the expectation values $\langle \hat{S}_z \rangle = \langle \hat{N}_\uparrow \rangle - N/2$. To measure the fidelity, we distinguish the single state with all ions in $|\downarrow\rangle$, which does not scatter from the cooling laser, from all other states. Any ion fluorescence indicates the system is no longer in the initial state. The fidelity is the fraction of experimental trials that result in measuring the state $|\downarrow \ldots \downarrow\rangle$ (see Supplementary Information).

Figure 3 shows the measured fidelity $\mathcal{F}$ as a function of the angle ϕ for different evolution times τ in an array of 48 ions. The measurements at $\phi = 0$ and 2π give the state purity, while the π-periodic oscillations encode information on the buildup of MQCs. The pulse sequence in Fig. 3a follows Fig. 1, whereas in Fig. 3b, an additional π-rotation has been inserted in the middle of each evolution period τ to suppress some forms of decoherence. We extract the coherences I_m, shown in Fig. 3c, as the Fourier components of the fidelity in Fig. 3b. We see a clear buildup of the two-body (I_2), and then four-body (I_4) coherences with increasing interaction time. Odd components are zero within statistical error, consistent with the fact that the coherences are generated by the Ising interaction, which can be viewed as only flipping pairs of spins.

All the measurements are in good agreement with theory calculations (solid lines) that account for independently calibrated sources of decoherence. Off-resonant light scattering is the dominant decoherence mechanism in the system. Because the fidelity measures a projection onto a single many-body state, it decays with a rate approximately $N\Gamma$, where Γ is the single-particle decoherence rate. This causes a fast decay of I_0 as $\exp(-N\Gamma\tau)$. However, Fig. 3c shows that I_0 decays as $\exp(-N\Gamma\tau)I_0^{(\mathrm{pure})}$, where the algebraic decay $I_0^{(\mathrm{pure})} \approx 1/(1 + J^2\tau^2)$ (see Supplementary Section 3) signals the buildup of higher-order coherences seen also in the fully coherent case. Other sources of decoherence include slow drifts in the magnetic field[36] and COM mode frequency fluctuations, which the MQC can distinguish. Figure 3a reveals the degree to which the COM axial mode phonons cannot be decoupled from the spins due to uncertainty in the COM mode frequency ω_z. The impact of residual spin–phonon coupling, arising from fluctuations in ω_z, is more pronounced at $\phi = \pi$ than $\phi = 0$. In contrast, slow magnetic field noise causes a reduction of the fidelity around $\phi = 0(2\pi)$, but has no effect at $\phi = \pi$, allowing us to benchmark these two imperfections independently. For the data in Fig. 3b, where the sequence includes an additional π rotation to suppress errors from slow drifts in the magnetic field and COM mode frequency, the full theory collapses to a solution that includes only off-resonant light scattering as the sole decoherence mechanism (dashed line).

Single-body observables, like the collective magnetization, are much less sensitive to decoherence, and provide an alternative way to experimentally measure the sequential buildup of higher-order correlations induced by spin–spin interactions. In Fig. 4, we show

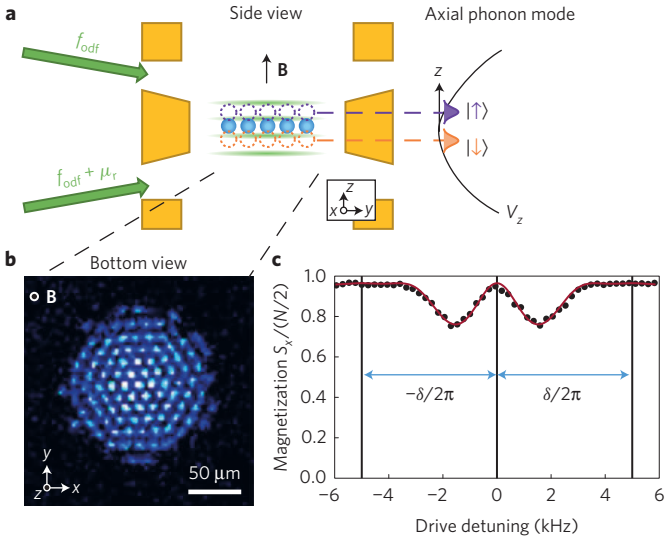

Figure 2 | Phonon-mediated, reversible spin–spin coupling in a Penning trap. a, (Left) Illustration of Penning trap cross-section. Ions (blue circles) are confined axially to a single 2D plane (shown in **b**) with static electric fields from potentials on the electrodes (gold). Rotation of the ions in the axial magnetic field **B** produces radial confinement from the Lorentz force. A pair of detuned ODF beams (green) interfere and form a travelling wave optical lattice, producing spin-dependent COM mode excitations that couple the spins to the axial phonon mode. Shown here are two of $(2N+1)$ excitations: all ions in $|\uparrow\rangle$ (purple) and all in $|\downarrow\rangle$ (orange). (Right) The phonon wave packets experience equal and opposite displacement in the axial potential V_z. Spin-dependent motion, along with the Coulomb interaction, generates the spin–spin coupling. **b**, Rotating frame image of 2D array of $^9Be^+$ ions, integration time 2.1 s. **c**, Residual spin–phonon coupling for drive frequencies away from the decoupling points $\pm\delta$ appears as a decrease in the magnetization measured after the experimental sequence from Fig. 1, with $\phi=\pi$, and without inverting $\hat{H}_{zz}$. Here $\tau=200\,\mu s$. Note that decoupling points appear at $\pm\delta$ with $+\delta$ giving an anti-ferromagnetic interaction, and $-\delta$ giving a ferromagnetic interaction used for the time reversal of the $\hat{H}_{zz}$ dynamics.

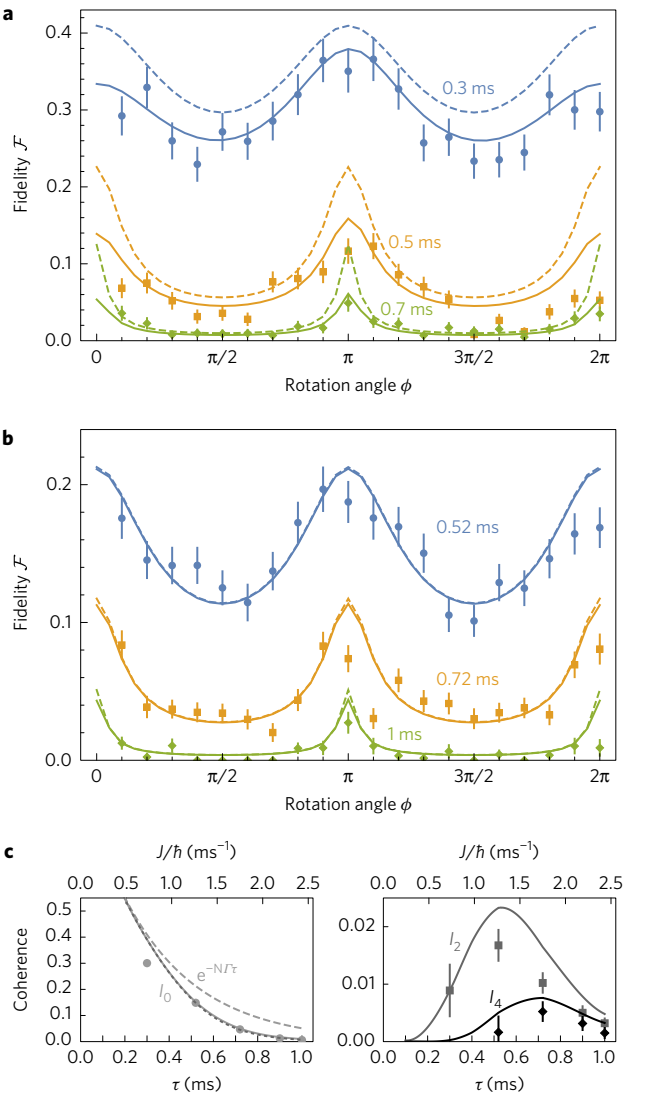

Figure 3 | Measured fidelity and coherence spectrum of $N=48$ ions. **a**,**b**, Dependence of the fidelity $\mathcal{F}_\phi(\tau)$ on the rotation angle ϕ. The experimental sequence in **b** includes an additional π pulse in the middle of each evolution period τ. The dashed lines are simulations including off-resonant light scattering as the only source of decoherence, with $\Gamma=62\,s^{-1}$. The solid lines include effects of COM mode and magnetic field fluctuations, with COM mode frequency fluctuations $\Delta_{COM}/\omega_z = 8.0\times10^{-5}$ r.m.s., and magnetic field noise $\Delta_B/B=0.32\times10^{-9}$ r.m.s. (Methods). Note that for each interaction time τ the detuning is chosen so that $\delta=2\pi/\tau$ (**a**) or $\delta=4\pi/\tau$ (**b**). In each case, the spin–spin coupling also varies as $J/\hbar=\Omega_0^2/(2\delta)$ where $\Omega_0=7{,}850\,s^{-1}$. **c**, Fourier amplitudes of fidelity (**b**) as a function of time. Solid lines are simulations including all known decoherence processes. I_2 and I_4 clearly show the buildup of higher-order MQCs. Odd coherences and coherences $m\geq6$ are zero within the statistical error. For I_0, decoherence induced decay (dashed) and approximate analytic curve (dotted, see text) are shown. The data points at $\tau=0.3$ and 0.9 (not shown in **b**) have been added. The longest measured evolution time of $\tau=1$ ms corresponds to 6.5% of t_{cat} (see Fig. 1d). All error bars denote the statistical error of 1 standard deviation (s.d.) of the mean.

the results of the magnetization OTOC measurement sequence, which shows a buildup of Fourier amplitudes, A_m, up to $m=8$, observable even for $N=111$. These measurements also allow us to benchmark the quality of our quantum simulator by comparing to theory predictions with no adjusted parameters. Here, the dashed lines are obtained by solving the pure spin model including only spontaneous emission decoherence (see Supplementary Information), showing agreement in both the ϕ-dependent signal (Fig. 4a) and its Fourier transform (Fig. 4b). Accounting for static magnetic field noise largely explains the remaining discrepancy at small angles (solid lines in Fig. 4a). Comparison of the data to theory predictions with no decoherence (Fig. 4c) confirms that the decay of the Fourier amplitudes at long times is not a decoherence effect but a consequence of many-body interactions which induce a decrease of low-m components with a corresponding buildup of high-m components. Since the observed dynamics is dominated by the coherent evolution under the Ising interaction, these results suggest that the observed features can be explained only by the formation of quantum correlations.

In summary, we have shown that many-body Loschmidt echo sequences are powerful tools to measure OTOCs and quantify the degree of coherence in quantum simulators, with an explicit demonstration for ions in a Penning trap. In particular, we studied OTOCs involving variable angle spin rotations. The Fourier components with respect to the rotation angle (I_m and A_m) show a buildup of many-body coherence and correlations, indicating scrambling of quantum information. Our experimental results are described well by a theory model which accounts for all known sources of decoherence (photon scattering, magnetic field noise, and spin–phonon coupling), allowing us to benchmark the performance of our trapped-ion quantum simulator.

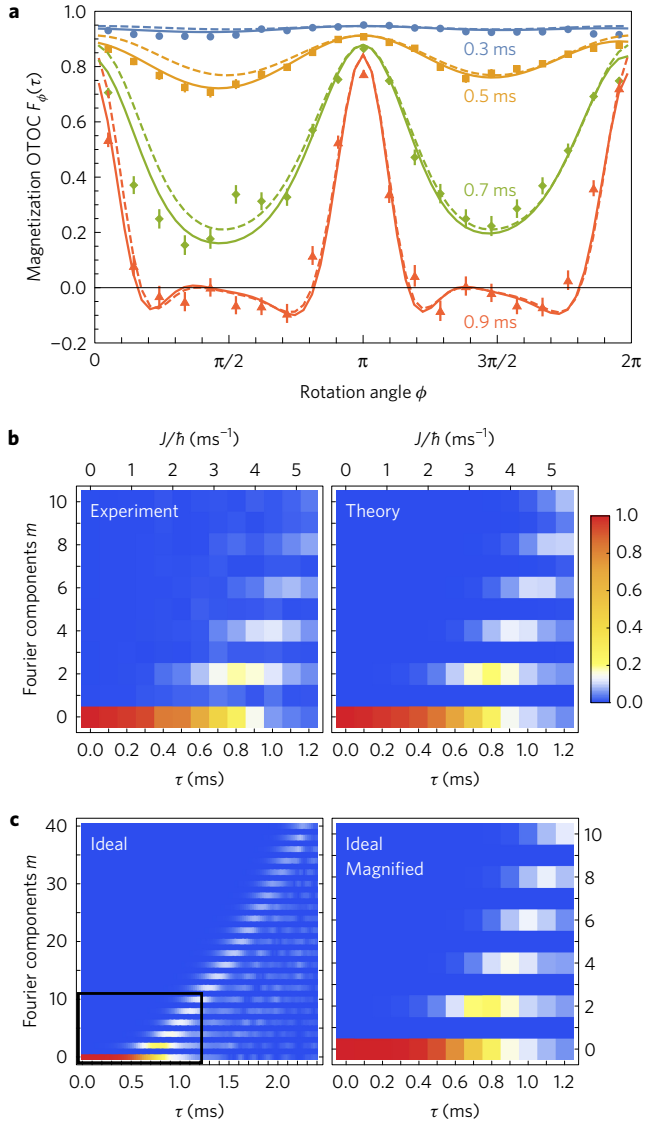

Figure 4 | Probing scrambling through magnetization dynamics. **a**, Dependence of the normalized component $F_\phi(\tau) = (2/N)\langle \hat{S}_x \rangle$ of the total spin on the rotation angle ϕ, measured in an array of $N = 111(2)$ ions. Lines are the solutions of the full master equation with (solid) and without (dashed) magnetic field noise, where $\Delta_B/B = 0.32 \times 10^{-9}$ r.m.s. The effect of COM mode fluctuations is negligible here. Error bars denote the statistical error of 1 s.d. of the mean. **b**, Fourier amplitudes A_m as a function of time. In the theory plot, the case without magnetic field noise (dashed lines in **a**) was used. The interaction parameter varies as $J/\hbar = \Omega_0^2/(2\delta)$ where $\Omega_0 = 7{,}450\ \mathrm{s}^{-1}$ and $\Gamma = 91\ \mathrm{s}^{-1}$. The longest measured evolution time of $\tau = 1.2$ ms corresponds to 7.3% of t_{cat}. **c**, Ideal case for $N = 111$, neglecting all decoherence effects. This corresponds to the lower panel of Fig. 1d. The box in the left panel shows the experimentally accessed region which is magnified in the right panel.

The characteristic features of A_ms reported in this work demonstrate a high level of control over the coherent many-body dynamics achieved by our trapped-ion quantum simulator and are fully consistent with the buildup of quantum correlations. Although currently the latter can be only indirectly inferred from the measurements, it is supported by previous benchmarking of the system using standard entanglement witnesses such as spin squeezing[18]. We expect future work to derive formal connections between entanglement and scrambling, and to construct strict bounds that witness entanglement directly from I_m and A_m measurements. Although the current experimental system realizes a model amenable to classical simulations, we envisage experiments going beyond this limit—for example, by adding a spatially inhomogeneous magnetic field or preparing the system in non-symmetric or impure initial states, such as thermal states. These generalizations will allow us to explore the dynamics of OTOCs and characterize scrambling in unexplored regimes and under conditions where fast scrambling can occur. Furthermore, the ability to time-reverse the dynamics will allow enhanced phase estimation without single-particle detection resolution[5,29,37], investigations of quantum phase transitions[38], criticality[39], thermalization in nearly closed quantum systems[13,40] and the exploration of the quantum-classical boundary[41]—for example, observation of the violation of Leggett–Garg inequalities[42].

After the completion of this work, we became aware of measurements of OTOCs using four spins in an NMR system[43].

Methods

Methods, including statements of data availability and any associated accession codes and references, are available in the online version of this paper.

Received 6 December 2016; accepted 30 March 2017; published online 22 May 2017

References

1. Loschmidt, J. Über den Zustand des Wärmegleichgewichtes eines Systems von Körpern mit Rücksicht auf die Schwerkraft. 1. Teil. *Sitzungsber. Kais. Akad. Wiss. Wien, Math. Naturwiss. Classe* **73,** 128–142 (1876).
2. Hahn, E. L. Spin echoes. *Phys. Rev.* **80,** 580–594 (1950).
3. Baum, J., Munowitz, M., Garroway, A. N. & Pines, A. Multiple-quantum dynamics in solid-state NMR. *J. Chem. Phys.* **83,** 2015–2025 (1985).
4. Widera, A. *et al*. Quantum spin dynamics of mode-squeezed Luttinger liquids in two-component atomic gases. *Phys. Rev. Lett.* **100,** 140401 (2008).
5. Linnemann, D. *et al*. Quantum-enhanced sensing based on time reversal of non-linear dynamics. *Phys. Rev. Lett.* **117,** 013001 (2016).
6. Swingle, B., Bentsen, G., Schleier-Smith, M. & Hayden, P. Measuring the scrambling of quantum information. *Phys. Rev. A* **94,** 040302 (2016).
7. Yao, N. Y. *et al*. Interferometric approach to probing fast scrambling. Preprint at http://arXiv.org/abs/1607.01801 (2016).
8. Shen, H., Zhang, P., Fan, R. & Zhai, H. Out-of-time-order correlation at a quantum phase transition. Preprint at http://arXiv.org/abs/1608.02438 (2016).
9. Zhu, G., Hafezi, M. & Grover, T. Measurement of many-body chaos using a quantum clock. *Phys. Rev. A* **94,** 062329 (2016).
10. Sekino, Y. & Susskind, L. Fast scramblers. *J. High Energy Phys.* **2008,** 065 (2008).
11. Shenker, S. H. & Stanford, D. Black holes and the butterfly effect. *J. High Energy Phys.* **2014,** 067 (2014).
12. Shenker, S. H. & Stanford, D. Stringy effects in scrambling. *J. High Energy Phys.* **2015,** 132 (2015).
13. Eisert, J., Friesdorf, M. & Gogolin, C. Quantum many-body systems out of equilibrium. *Nat. Phys.* **11,** 124–130 (2015).
14. Fu, W. & Sachdev, S. Numerical study of fermion and boson models with infinite-range random interactions. *Phys. Rev. B* **94,** 035135 (2016).
15. Danshita, I., Hanada, M. & Tezuka, M. Creating and probing the Sachdev-Ye-Kitaev model with ultracold gases: towards experimental studies of quantum gravity. Preprint at http://arXiv.org/abs/1606.02454 (2016).
16. Hosur, P., Qi, X.-L., Roberts, D. A. & Yoshida, B. Chaos in quantum channels. *J. High Energy Phys.* **2016,** 004 (2016).
17. Kitaev, A. A simple model of quantum holography (7 April 2015 and 27 May 2015). Talks given at The Kavli Institute for Theoretical Physics (KITP) (University of California).
18. Bohnet, J. G. *et al*. Quantum spin dynamics and entanglement generation with hundreds of trapped ions. *Science* **352,** 1297–1301 (2016).
19. Leibfried, D. *et al*. Creation of a six-atom 'Schrödinger cat' state. *Nature* **438,** 639–642 (2005).
20. Monz, T. *et al*. 14-qubit entanglement: creation and coherence. *Phys. Rev. Lett.* **106,** 130506 (2011).
21. Strobel, H. *et al*. Fisher information and entanglement of non-gaussian spin states. *Science* **345,** 424–427 (2014).
22. Álvarez, G. A., Suter, D. & Kaiser, R. Localization-delocalization transition in the dynamics of dipolar-coupled nuclear spins. *Science* **349,** 846–848 (2015).

23. Sánchez, C. M., Levstein, P. R., Acosta, R. H. & Chattah, A. K. NMR Loschmidt echoes as quantifiers of decoherence in interacting spin systems. *Phys. Rev. A* **80,** 012328 (2009).
24. Debnath, S. *et al*. Demonstration of a small programmable quantum computer with atomic qubits. *Nature* **536,** 63–66 (2016).
25. Cucchietti, F. M. Time reversal in an optical lattice. *J. Opt. Soc. Am. B* **27,** A30–A35 (2010).
26. Leroux, I. D., Schleier-Smith, M. H. & Vuletić, V. Implementation of cavity squeezing of a collective atomic spin. *Phys. Rev. Lett.* **104,** 073602 (2010).
27. Hosten, O., Krishnakumar, R., Engelsen, N. J. & Kasevich, M. A. Quantum phase magnification. *Science* **352,** 1552–1555 (2016).
28. Douglas, J. S. *et al*. Quantum many-body models with cold atoms coupled to photonic crystals. *Nat. Photon.* **9,** 326–331 (2015).
29. Macrí, T., Pezzé, L. & Smerzi, A. Loschmidt echo for quantum metrology. *Phys. Rev. A* **94,** 010102(R) (2016).
30. Houck, A. A., Tureci, H. E. & Koch, J. On-chip quantum simulation with superconducting circuits. *Nat. Phys.* **8,** 292–299 (2012).
31. Sørensen, A. & Mølmer, K. Quantum computation with ions in thermal motion. *Phys. Rev. Lett.* **82,** 1971–1974 (1999).
32. Britton, J. W. *et al*. Engineered two-dimensional Ising interactions in a trapped-ion quantum simulator with hundreds of spins. *Nature* **484,** 489–492 (2012).
33. Sawyer, B. C. *et al*. Spectroscopy and thermometry of drumhead modes in a mesoscopic trapped-ion crystal using entanglement. *Phys. Rev. Lett.* **108,** 213003 (2012).
34. Biercuk, M. J. *et al*. High-fidelity quantum control using ion crystals in a Penning trap. *Quant. Info. Comput.* **9,** 920–949 (2009).
35. Leibfried, D. *et al*. Experimental demonstration of a robust, high-fidelity geometric two ion-qubit phase gate. *Nature* **422,** 412–415 (2003).
36. Britton, J. W. *et al*. Vibration-induced field fluctuations in a superconducting magnet. *Phys. Rev. A* **93,** 062511 (2016).
37. Davis, E., Bentsen, G. & Schleier-Smith, M. Approaching the Heisenberg limit without single-particle detection. *Phys. Rev. Lett.* **116,** 053601 (2016).
38. Cucchietti, F. M., Fernandez-Vidal, S. & Paz, J. P. Universal decoherence induced by an environmental quantum phase transition. *Phys. Rev. A* **75,** 032337 (2007).
39. Quan, H. T., Song, Z., Liu, X. F., Zanardi, P. & Sun, C. P. Decay of Loschmidt echo enhanced by quantum criticality. *Phys. Rev. Lett.* **96,** 140604 (2006).
40. Nandkishore, R. & Huse, D. A. Many-body localization and thermalization in quantum statistical mechanics. *Annu. Rev. Condens. Matter Phys.* **6,** 15–38 (2015).
41. Jacquod, P. & Petitjean, C. Decoherence, entanglement and irreversibility in quantum dynamical systems with few degrees of freedom. *Adv. Phys.* **58,** 67–196 (2009).
42. Fröwis, F., Sekatski, P. & Dür, W. Detecting large quantum Fisher information with finite measurement precision. *Phys. Rev. Lett.* **116,** 090801 (2016).
43. Li, J. *et al*. Measuring out-of-time-order correlators on a nuclear magnetic resonance quantum simulator scrambling. Preprint at http://arXiv.org/abs/1609.01246 (2016).

Acknowledgements

We thank P. Hauke, J. Price and S. Kolkowitz for discussions and careful reading of our manuscript, and gratefully acknowledge J. Britton and B. Sawyer for preceding experimental contributions to this work. Supported by Defense Advanced Research Projects Agency (DARPA) ATN program through grant number W911NF-16-1-0576 through the Army Research Office (ARO), NSF grant PHY 1521080, JILA-NSF grant PFC-1125844, the ARO, and the Air Force Office of Scientific Research and its Multidisciplinary University Research Initiative (AFOSR-MURI) (A.M.R.) and by a National Research Council Research Associateship Award at NIST (J.G.B. and M.L.W.). All authors acknowledge financial support from NIST.

Author contributions

J.G.B. and J.J.B. conducted the experiment. The theoretical modelling was done by M.G., A.S.-N., M.L.W. and A.M.R. All authors jointly interpreted and discussed the experimental data.

Additional information

Supplementary information is available in the online version of the paper. Reprints and permissions information is available online at www.nature.com/reprints. Publisher's note: Springer Nature remains neutral with regard to jurisdictional claims in published maps and institutional affiliations. Correspondence and requests for materials should be addressed to A.M.R.

Competing financial interests

The authors declare no competing financial interests.

Methods

Trap parameters. The experimental system is a two-dimensional (2D) Wigner crystal of $^9Be^+$ ions formed in a Penning trap, described in ref. 18. Details relevant to this work are documented here. Axial confinement in the trap is provided by electric potentials applied to a stack of cylindrical electrodes; radial confinement is achieved using the Lorentz force produced by the controlled ion crystal rotation through the axial magnetic field, $B = 4.46$ T, of the trap. The axial trap frequency is $\omega_z = 1.570$ MHz, with a rotation frequency of $\omega_r = 180$ kHz. The ions are laser-cooled to the Doppler limit ($\approx$0.5 mK, with mean thermal occupation $\bar{n} \approx 6$) using a pair of beams tuned close to the optical cycling transition $|^2S_{1/2}J = +1/2, m_J = 1/2\rangle \rightarrow |^2P_{3/2}J = +3/2, m_J = 3/2\rangle$. The centre-of-mass (COM) motional mode frequency is the trap axial frequency ω_z, with the shorter wavelength modes well-resolved at lower frequencies[33].

Qubit parameters. The two-level spin system is formed by the valence electron spin in the magnetic field of the Penning trap, with $|\uparrow\rangle = |m_J = 1/2\rangle$ ($|\downarrow\rangle = |m_J = -1/2\rangle$) parallel (anti-parallel) to the field. The spin states are split by 124 GHz. Global spin state rotations are performed using resonant microwaves, characterized by a π rotation time of 70 µs. The coherence time is primarily limited by shot-to-shot magnetic field fluctuations, causing fluctuations of the qubit state splitting with a standard deviation of 40 Hz.

Effective Hamiltonian parameters. The Ising Hamiltonian evolution is implemented using the spin–motion coupling described in equation (6). The spin-dependent ODF, with magnitude $|F_0| = |\hbar\Omega_0|/z_0$, where $z_0 \equiv \sqrt{\hbar/(2m\omega_z)}$ is the ground state wavefunction size for a single trapped ion, is provided by a pair of far-detuned 313 nm laser beams that excite the axial drumhead modes of the ion crystal. The Coulomb force mediates effective spin–spin interactions through the spin-dependent motion, leading to well-characterized Ising interactions[18,32], similar to those used in a number of trapped-ion quantum simulators[44–46]. For this work, $|F_0|$ is typically 45 yN. The detuning δ in this work ranges from $2\pi\times1$ kHz to $2\pi\times5$ kHz, and the impact of coupling to other axial modes, separated by at least $2\pi\times25$ kHz from ω_z, is negligible. For $\delta = 2\pi\times1$ kHz, we typically achieve $J/\hbar$ between 4,000 and 5,000 s^{-1}, calibrated using mean-field spin precession[32] and collective spin depolarization[18].

Decoherence. The ODF beams scatter off-resonant photons, which is the primary source of decoherence during the coherent evolution. We independently determine the total single-particle decoherence rate Γ using measurements of the decay of the second-order moment of the collective spin $\langle\hat{\mathbf{S}}^2\rangle$. Typically, $\Gamma \sim 65\,s^{-1}$, in good agreement with the prediction from the laser intensity alone. However, for the data in Fig. 4, we measured $\Gamma \sim 90\,s^{-1}$, which we attribute to effects of the larger Lamb–Dicke confinement parameter for this data (see Supplementary Information of ref. 18), which had tighter radial trapping parameters than the data in Fig. 3 (and therefore lower frequency transverse modes). The decoherence rate Γ is dominated by elastic Rayleigh scattering, which is 3.9 times the total inelastic Raman scattering rate[47].

Beyond spontaneous emission, we also observe effects of fluctuations in the trap axial frequency ω_z. Any fluctuations in the COM frequency will adversely affect the final state fidelity, since entanglement between the spin and motional degrees of freedom is present unless operating precisely at the decoupling times τ_n. In addition, errors in δ lead to different spin–spin couplings in the two halves of the echo sequence, leading to imperfect many-body echoes (Supplementary Information). We independently measure the effective COM mode stability with an experimental sequence like that of Fig. 1 with $\phi = \pi$, and δ is nominally set to zero, measuring $\langle\hat{S}_x\rangle$ versus τ. From the decay of $\langle\hat{S}_x\rangle$, we find the effective r.m.s. fluctuations in ω_z to be $2\pi\times125(50)$ Hz. The incorporation of the COM mode frequency fluctuations in our theoretical model is described in a later section.

We measure shot-to-shot magnetic field fluctuations using the experimental sequence of Fig. 1, but with the ODF beams blocked and $\phi = 0$. From the decay of $\langle\hat{S}_x\rangle$ versus τ, we determined magnetic-field-induced fluctuations in the qubit frequency of 40 Hz r.m.s. We note that these measured fluctuations are the same order as, but slightly smaller than measured previously ($\sim$68 Hz; ref. 36).

Experimental readout. To measure the fidelity, we distinguish the single state with all ions in $|\downarrow\rangle$, which does not scatter from the cooling laser, from all other states. Off-resonant repumping from the cooling laser limits the detection time, and so setting a photon count threshold based on the average photons collected per ion generally underestimates the fidelity $\mathcal{F}_\phi$. We recover nearly all the fidelity using a reference photon count distribution where all ions are prepared in $|\downarrow\rangle$ (Supplementary Information).

Multiple quantum coherence protocol. To prove the relation between the Fourier components of the fidelity and the multiple quantum intensities (or coherences) I_m we introduce the canonical product basis $|\boldsymbol{\alpha}\rangle = |\alpha_1 \ldots \alpha_N\rangle$, where $\alpha_i \in \{+,-\}$ and $|\pm\rangle$ are the eigenstates of $\hat{\sigma}_x$. The states $|\boldsymbol{\alpha}\rangle$ are eigenstates of $\hat{S}_x = \sum_i \hat{\sigma}_i^x/2$ with eigenvalues M_x, which are (half) integer numbers between $-N/2$ and $N/2$. We can now write the state $\hat{\rho}(\tau)$ as a sum of different coherence sectors $\hat{\rho}(\tau) = \sum_m \hat{\rho}_m$. Here, $\hat{\rho}_m$ contains all density matrix elements that account for coherences between basis states $|\boldsymbol{\alpha}\rangle$ and $|\boldsymbol{\alpha}'\rangle$ for which $M_x - M_x' = m$; that is, which differ in the number of spins in the $|+\rangle$-state by m.

With this, one defines the MQC spectrum known from NMR[3]:

$$I_m = \mathrm{tr}[\hat{\rho}_m\hat{\rho}_{-m}] = \sum_{M_x - M_{x'} = m} |\hat{\rho}_{\boldsymbol{\alpha}\boldsymbol{\alpha}'}|^2 \tag{7}$$

Noting that a rotation about x only results in the mth sector picking up a phase $-m\phi$, one finds

$$\begin{aligned}\mathcal{F}_\phi(\tau) &= \mathrm{tr}[\hat{\rho}_0\hat{\rho}_f] = \mathrm{tr}[\hat{\rho}_0\hat{\mathcal{U}}^\dagger R_x(\phi)\hat{\mathcal{U}}\hat{\rho}_0\hat{\mathcal{U}}^\dagger\hat{R}_x^\dagger(\phi)\hat{\mathcal{U}}] \\ &= \mathrm{tr}[\hat{\rho}(\tau)\hat{\rho}_\phi(\tau)] = \mathrm{tr}\left[\sum_{m'}\hat{\rho}_{m'}\sum_m\hat{\rho}_m e^{-im\phi}\right] \\ &= \sum_m \mathrm{tr}[\hat{\rho}_{-m}\hat{\rho}_m]e^{-im\phi} = \sum_m I_m e^{-im\phi}\end{aligned} \tag{8}$$

where $\hat{\rho}_\phi(\tau) = \hat{R}_x(\phi)\hat{\rho}(\tau)\hat{R}_x^\dagger(\phi)$ and $\hat{\mathcal{U}} = \exp[-i\hat{H}_{zz}\tau]$, and we have used cyclic permutations under the trace. The equality $\mathcal{F}_\phi(\tau) = \mathrm{tr}[\hat{\rho}(\tau)\hat{\rho}_\phi(\tau)]$ shows that for $\phi = 0$ the fidelity measures the purity of the state $\hat{\rho}(\tau)$. Equation (8) still holds in the presence of specific types of decoherence present in our experiment (Supplementary Information).

Scrambling of quantum information from Ising models. In this section we provide further insight on the scrambling of quantum information. We show that the mth Fourier component of $F_\phi(\tau)$ is non-zero only if at least one expectation value of an n-point operator, with $n \geq m$, is non-zero. Details of this calculation can be found in the Supplementary Information.

In the main text we defined the magnetization OTOC as the x-magnetization per spin $F_\phi(\tau) = (2/N)\langle\hat{S}_x\rangle = 1/N\sum_{i=1}^N\langle\hat{\sigma}_i^x\rangle$, which with permutation symmetry simplifies to $F_\phi(\tau) = \langle\hat{\sigma}_i^x\rangle$ (for any i). We can express the global magnetization $\langle\hat{S}^x\rangle$ at the end of the time-reversal scheme in terms of an expectation value in $\hat{\rho}(\tau)$ (analogous to equation equation (8)): $\langle\hat{S}^x\rangle = \mathrm{tr}[\hat{R}_x(\phi)\hat{\mathcal{U}}\hat{S}^x\hat{\mathcal{U}}^\dagger\hat{R}_x^\dagger(\phi)\hat{\rho}(\tau)]$, where $\hat{\mathcal{U}}$ is the unitary evolution under the interaction Hamiltonian, $\hat{R}_x(\phi)$ generates the rotation of the spins about x. Thus, $\langle\hat{S}^x\rangle$ has the form $\langle e^{-i\hat{S}^x\phi}\hat{O}(\tau)e^{i\hat{S}^x\phi}\rangle_\tau$, where $\langle\cdot\rangle_\tau$ denotes the expectation value in state $\hat{\rho}(\tau)$. The general Hermitian operator $\hat{O}(\tau)$ can be written as a sum of products of single-spin operators $\hat{O}(\tau) = \sum_k a_k\prod_{j\in D_k}\hat{\sigma}_j^{b_j^k}$, where $D_k \subset \{1,\ldots,N\}$ is a set of particle indices and $b_j^k \in \{x,y,z\}$. Applying the x-rotation to the operator $\hat{O}(\tau)$ is accomplished by replacing all Pauli spin operators according to: $\hat{\sigma}^x \rightarrow \hat{\sigma}^x$, $\hat{\sigma}^y \rightarrow \hat{\sigma}^y\cos(\phi) + \hat{\sigma}^z\sin(\phi)$, and $\hat{\sigma}^y \rightarrow \hat{\sigma}^z\cos(\phi) - \hat{\sigma}^y\sin(\phi)$. The resulting operator can be restated as

$$\begin{aligned}\langle e^{-i\hat{S}_x\phi}\hat{O}(\tau)e^{i\hat{S}_x\phi}\rangle_\tau &= \left\langle\sum_k\tilde{a}_k(\cos\phi)^{p_k}(\sin\phi)^{q_k}\prod_{j\in\tilde{D}_k}\hat{\sigma}_j^{\tilde{b}_j^k}\right\rangle_\tau \\ &= \sum_k\tilde{a}_k(\cos\phi)^{p_k}(\sin\phi)^{q_k}\langle\hat{\mathcal{C}}_{\tilde{D}_k}\rangle_\tau\end{aligned} \tag{9}$$

Here the tilde indicates that the coefficients and indices are different from the ones of $\hat{O}(\tau)$. p_k and q_k satisfy $0 \leq p_k + q_k \leq N$. The crucial step is now to notice that terms with $p_k + q_k = m$ are associated with at least m-spin correlation functions, that is, expectation values $\langle\hat{\mathcal{C}}_{\tilde{D}_k}\rangle$ of products of $|D_k| \geq m$ spin Pauli spin operators. Expanding $\langle e^{-i\hat{S}_x\phi}\hat{O}(\tau)e^{i\hat{S}_x\phi}\rangle$ into a Fourier series we find that terms with $p_k + q_k = m$ contribute only to Fourier components A_n where $n \leq m$. Thus, if all correlation functions of more than m spins are zero, then also all Fourier components above m necessarily vanish. Conversely, if we observe a Fourier component $|A_m| > 0$, we know that n-body correlations with $n \geq m$ must exist.

In the Supplementary Information we illustrate this argument by considering the concrete case of an Ising model with arbitrary couplings J_{ij}. We show that for a k-local Ising model, in which any spin interacts with at most k others, only Fourier components A_m with $m \leq k+1$ can appear. For example, in a one-dimensional Ising chain with nearest-neighbour interactions, no higher components than A_3 can buildup. In addition, the successive buildup of higher A_m as a function of time τ and the vanishing of odd components can be understood in this way.

The observation of higher-order Fourier components of $F_\phi(\tau)$ also allows to draw conclusions about the unitary evolution that creates the interacting dynamics. If this unitary is fully separable—that is, a product of unitaries acting on single spins, such as a simple rotation—then $F_\phi(\tau)$ can at most develop Fourier components $|m| \leq 1$, since in this case $\langle\hat{S}_x\rangle$ can be written as a sum of independent single-particle expectation values. This argument can be generalized to unitaries

being products of terms acting on disjoint subsets of spins of at most size $\leq m$. If this is the case, then $A_{n>m}=0$. Thus, the observation of non-zero A_m implies that the interaction Hamiltonian couples clusters of at least m spins. We emphasize that this result is general, and does not rely on the assumption of an Ising interaction.

In the main text we noted that $\langle|[\hat{W}(\tau),\hat{V}]|^2\rangle = 2(1-\mathrm{Re}[F(\tau)])$. This holds if both $\hat{W}(\tau)$ and $\hat{V}$ are unitary (as for $\hat{W}(\tau)=\hat{W}_\phi(\tau)=\exp(\mathrm{i}\hat{H}\tau)\hat{R}_x(\phi)\exp(-\mathrm{i}\hat{H}\tau)$ and $\hat{V}=\hat{\sigma}_i^x$). If $\hat{V}=\hat{\rho}_0=|\psi_0\rangle\langle\psi_0|$ is the projector in the (pure) initial state, we obtain

$$\langle|[\hat{W}(\tau),\hat{V}]|^2\rangle = 1-\langle\hat{W}^\dagger(\tau)\hat{V}\hat{W}(\tau)\hat{V}\rangle = 1-\mathcal{F}_\phi(\tau) \tag{10}$$

where we used that $\hat{V}=\hat{V}^\dagger$, $\hat{V}^2=\hat{V}$ and $\hat{V}|\psi_0\rangle=|\psi_0\rangle$.

Data availability. The data that support the plots within this paper and other findings of this study are available from the corresponding author upon reasonable request.

References

44. Porras, D. & Cirac, J. I. Effective quantum spin systems with trapped ions. *Phys. Rev. Lett.* **92,** 207901 (2004).
45. Richerme, P. *et al*. Non-local propagation of correlations in quantum systems with long-range interactions. *Nature* **511,** 198–201 (2014).
46. Jurcevic, P. *et al*. Quasiparticle engineering and entanglement propagation in a quantum many-body system. *Nature* **511,** 202–205 (2014).
47. Uys, H. *et al*. Decoherence due to elastic Rayleigh scattering. *Phys. Rev. Lett.* **105,** 200401 (2010).